Experimental Study of Trapped-Electron-Mode Properties in Tokamaks: Threshold and Stabilization by Collisions

F. Ryter, C. Angioni, A. G. Peeters, F. Leuterer, H.-U. Fahrbach, W. Suttrop, and ASDEX Upgrade Team
Max-Planck-Institut für Plasmaphysik, EURATOM Association, D-85748 Garching, Germany
(Received 6 April 2005; published 16 August 2005)

Trapped electron modes are one of the candidates to explain turbulence driven electron heat transport observed in tokamaks. This instability has two characteristics: a threshold in normalized gradient and stabilization by collisions. Experiments using modulated electron cyclotron heating in the ASDEX Upgrade tokamak demonstrate explicitly the existence of the threshold. The stabilization with increasing collisionality is evidenced by a strong decrease of the propagation of heat pulses, explained by a transition to ion temperature gradient driven transport. These results are supported by linear gyrokinetic calculations.

DOI: 10.1103/PhysRevLett.95.085001 PACS numbers: 52.55.Fa, 52.25.Fi

Understanding cross-field heat transport in tokamaks is crucial for future fusion devices. For more than two decades the electron temperature profiles T_e in tokamaks have been observed to be remarkably insensitive to changes of the auxiliary heating power deposition profile [1–8]. Experiments suggest that electron heat transport is governed by turbulence increasing above a threshold in a normalized gradient $R/L_{T_e} = -R\nabla T_e/T_e$, R being the major radius [9–15]. In addition to diffusion caused by collisional processes, heat transport in fusion plasmas is attributed to microturbulence, see, e.g., [16], which dominates by 1 or 2 orders of magnitude for electrons. Possible candidates able to drive electron heat transport include trapped electron modes (TEM), electron temperature gradient modes (ETG), and to a lesser extent, ion temperature gradient modes (ITG). The TEM and ITG are in the "long" wavelength range with $k_\theta \rho_s \simeq 0.3$, whereas the ETG have short wavelengths with $k_\theta \rho_s \simeq 10$, k_θ being the poloidal wave number of the unstable modes and $\rho_s = \sqrt{m_i T_e}/(eB)$ the ion Larmor radius with electron temperature. These three types of modes are unstable above their respective thresholds and their contribution to electron heat transport can be comparable or one type can dominate, depending on the conditions. The TEM threshold depends on several parameters such as R/L_{T_e}, normalized density gradient R/L_n, safety factor q, and magnetic shear $\hat{s}$, [17]. In addition, TEM modes are predicted to be gradually stabilized by increasing collisionality, the relevant quantity being $\nu_{\rm eff} \propto \nu_{ei}/\omega_{D_e}$, the ratio of electron-ion collision frequency to curvature drift frequency [18]. The ITG threshold is essentially in R/L_{T_i} and its stability does not depend upon collisions. The ETG threshold is given by the formula derived in [19], which indicates, in particular, that for usual tokamak plasma parameters, the ETG becomes unstable if T_e is close to or lower than T_i. In plasmas with dominant electron heating provided by electron cyclotron heating (ECH) having $T_e > T_i$ and low $\nu_{\rm eff}$, the TEM modes dominate; the ETG modes are stable [17]. Therefore, in such cases, the TEM properties can be studied under clear conditions. The present work provides direct experimental evidence for two main properties of the TEMs: threshold in R/L_{T_e} and stabilization by collisions.

At ASDEX Upgrade, experiments to vary R/L_{T_e} while keeping T_e almost constant were carried out using on-axis and off-axis ECH [15]. The results point towards a finite value of R/L_{T_e} as the electron heat flux q_e tends to zero, suggesting the existence of a threshold. Comparison of these results with GS2 linear gyrokinetic calculations confirms that heat transport is dominated by TEM and shows good agreement of the heat flux dependence upon R/L_{T_e}, including the existence of a threshold [17]. Similar experiments repeated recently in the tokamaks DIII-D [20] and TCV [21] yield similar results. However, none of these results could *explicitly* show the threshold $R/L_{T_{cr}}$ because R/L_{T_e} could not be reduced below this value, even with full off-axis ECH deposition. This is attributed to the fact that, close to the threshold, transport is low and the residual ohmic heating power can sustain the T_e profile just above $R/L_{T_{cr}}$. To reduce the residual ohmic power and reach lower values of R/L_{T_e}, new experiments were carried out in the ASDEX Upgrade and presented here.

The most complete investigations of transport are obtained when analyses from power balance and transient phenomena are carried out simultaneously [22]. Power modulation of ECH is particularly suited for transient studies of electron heat transport. The analysis of the induced temperature modulation $\tilde{T}_e$ yields the experimental heat pulse (HP) diffusivity $\chi_e^{\rm HP}$ which is the slope of the heat flux q_e versus $n_e\nabla T_e$, at the time-averaged working point [22]. This quantity differs from the power balance (PB) diffusivity $\chi_e^{\rm PB} = q_e/(n_e\nabla T_e)$. The standard method provides $\chi_e^{\rm HP} = \sqrt{\chi_e^{\rm amp}\chi_e^{\rm phase}}$, where $\chi_e^{\rm amp}$ and $\chi_e^{\rm phase}$ are deduced from the amplitude and phase profiles yielded by the Fourier transform of $\tilde{T}_e$, [22]. As pointed out in [23] $\chi_e^{\rm HP}$ is expected to exhibit a jumplike increase at the threshold when R/L_{T_e} is scanned. Even if transport below the threshold is not strictly zero, a nonlinear behavior of q_e as a function of R/L_{T_e} around the threshold is reflected in $\chi_e^{\rm HP}$.

A simple empirical model for electron heat transport assuming the existence of $R/L_{T_{cr}}$ can be written as, [24], $\chi_e = q^{3/2}\frac{T_e}{(eB)}\frac{\rho_s}{R}[\chi_s(\frac{R}{L_{T_e}} - \frac{R}{L_{T_{cr}}})^\alpha + \chi_0]$ above the threshold and $\chi_e = q^{3/2}\frac{T_e}{(eB)}\frac{\rho_s}{R}\chi_0$ below it. The dimensionless coefficients χ_s, χ_0, $R/L_{T_{cr}}$, and α are adjusted. The factor $\frac{T_e}{(eB)}\frac{\rho_s}{R}$ expresses the gyro-Bohm dependence expected for microturbulence which introduces a $T_e^{3/2}$ dependence. The model has been applied successfully, in general with $\alpha = 1$, to reproduce ASDEX Upgrade data [15,23] and for intermachine comparisons [24]. Above the threshold, q_e has a quadratic dependence in R/L_{T_e} for $\alpha = 1$ and weaker than quadratic for $\alpha < 1$. Here we applied the empirical model with $\alpha = 1.0$ and $\alpha = 0.8$ using the transport code ASTRA [25]. The calculations take into account the required experimental data including the ECH power deposition profiles and modulation properties. The simulations include the electron-ion energy exchange term, ohmic power, effective ion charge, and radiation losses, the latter being negligible in the core. These simulations yield the modulation of the electron temperature profile as a function of time, from which we take the Fourier transform and deduce $\chi_e^{\text{amp,sim}}$ and $\chi_e^{\text{phase,sim}}$ in the same way done for the experimental T_e. We also analyze the stability of the modes driving the microturbulence with the GS2 gyrokinetic code [26].

To reduce the residual ohmic power, the experiments presented here were carried out at low plasma current, $I_p = 400$ kA instead of 800 kA as in our previous experiments [15]. The magnetic field was about 2.2 T, resulting in the edge safety factor of $q_{95} \approx 8$. The measurements are made with the usual diagnostics available on a tokamak. In particular, T_e is measured by a 60 channel electron cyclotron emission (ECE) radiometer, sampled at 32 kHz. Similarly to our previous studies, [15], the value of R/L_{T_e} was varied by changing the ratio of the power $P_{\text{ECH}_{\text{in}}}$ and $P_{\text{ECH}_{\text{out}}}$ of two ECH beams, while keeping the total power constant, at about 0.65 MW in this case. The beams ECH_{in} and ECH_{out} were deposited at $\rho_{\text{ECH}_{\text{in}}} = 0.35$ and $\rho_{\text{ECH}_{\text{out}}} = 0.55$, ρ being the normalized toroidal flux radius. The analyses were made at $\rho \approx 0.45$. The line average electron density $\bar{n}_e \approx 2 \times 10^{19}$ m^{-3} was low to guarantee low collisionality and weak coupling between the ion and electron channels. These conditions provide $T_e \geq 1.3T_i$ and low ion heat flux. The power modulation, made at 30 Hz on $P_{\text{ECH}_{\text{out}}}$, was about $\pm 10\%$ of the total ECH power and the induced $\tilde{T}_e$ remained a small perturbation. The rather high q_{95} value keeps sawtooth amplitude and inversion radius small and the sawtooth induced heat pulses do not perturb the modulation analysis.

The experimental results are given in Fig. 1. The experimental heat flux exhibits indeed a clear change of slope at $R/L_{T_e} \approx 3$. The values of $P_{\text{ECH}_{\text{in}}}$ are indicated in the figure to show the fine heat flux scan required at low values of R/L_{T_e}. For low values of $P_{\text{ECH}_{\text{in}}}$, the experimental uncertainties on q_e are dominated by those on T_i, whereas at high values of $P_{\text{ECH}_{\text{in}}}$ they are determined by those on $P_{\text{ECH}_{\text{in}}}$, as reflected by the error bars in Fig. 1. The simulations using the empirical transport model with $\alpha = 1.0$ and $\alpha = 0.8$ were performed with constant $R/L_{T_{cr}}$ and χ_0, adjusting only χ_s to have good agreement with the experiment around the threshold and at the upper boundary of the R/L_{T_e} range. As expected, for $\alpha = 1.0$ the quadratic dependence of q_e is somewhat more curved than for $\alpha = 0.8$. The results with $\alpha = 0.8$ are somewhat closer to the experimental points. The line indicates the growth rate γ of the TEM, taken at the maximum of $\gamma/k_\perp^2$, as yielded by linear GS2 calculations for conditions in agreement with the experimental values within their uncertainties. The values of $k_\theta \rho_i$ decrease from 0.2–0.18 as γ increases in the range shown in Fig. 1. Comparisons between linear and nonlinear calculations for the TEM modes indicate that, unlike the simulation for ITG turbulence, linear and nonlinear gyrokinetic calculations yield very similar results [27]. It is explicitly shown that for TEMs zonal flows have a weak influence. In the same work it is also shown that the growth rate of the TEM corresponding to the maximum of $\gamma/k_\perp^2$ represents at best electron heat transport. Therefore, the threshold indicated by our linear calculations is expected to be close to the actual threshold. The GS2 calculations suggest that below the threshold the ITG may drive the residual heat flux. However, neither the experimental accuracy nor these linear calculations allow for a clear statement on the character of the residual electron heat

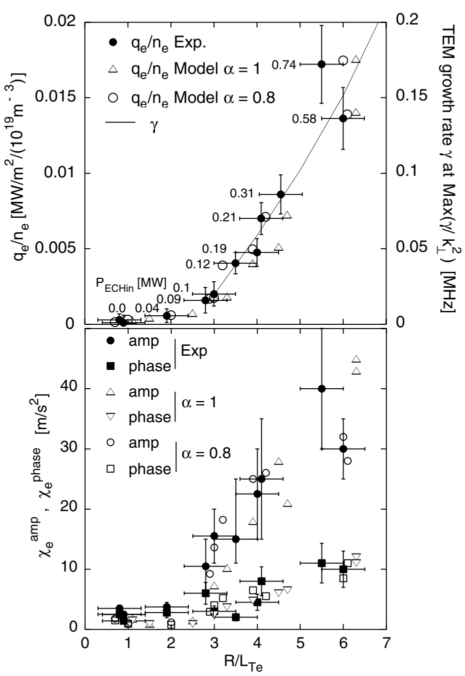

FIG. 1. Upper plot: electron heat flux versus R/L_{T_e}, experimental data, and simulations with the empirical model. The line indicates the growth rate of the TEM at the maximum of $\gamma/k_\perp^2$. Lower plot: χ_e^{amp} and χ_e^{phase} versus R/L_{T_e}. Experimental data and results from modeling as indicated by the legend.

flux below the threshold. In the lower plot of Fig. 1 the behavior of χ_e^{amp} exhibits a clear jump at $R/L_{T_e} \approx 3$, corresponding to the change of slope in q_e. Below this value χ_e^{amp} and χ_e^{phase} are similar and at low value. Above $R/L_{T_e} \approx 3$ both quantities increase, χ_e^{amp} stronger than χ_e^{phase}. This behavior is caused by the change of $\partial q_e/(n_e \partial \nabla T_e)$ and interpreted as a threshold. For purely diffusive transport one would expect $\chi_e^{\mathrm{amp}} \leq \chi_e^{\mathrm{phase}}$, the difference being due to damping [22]. The situation $\chi_e^{\mathrm{amp}} > \chi_e^{\mathrm{phase}}$ observed here for $R/L_{T_e} > 3$ is an additional signature for the existence of the threshold. In fact, if $R/L_{T_e} > R/L_{T_{cr}}$ the heat pulses excited by $\mathrm{ECH_{out}}$ and propagating toward the center reach a region around $\mathrm{ECH_{in}}$ where R/L_{T_e} drops below the threshold. Therefore, each heat pulse arriving there will cause a modulation of R/L_{T_e} around the threshold where $P_{\mathrm{ECH_{in}}}$ is deposited. This cyclic change of transport in a region with a high and localized power density provided by $P_{\mathrm{ECH_{in}}}$ excites a secondary heat wave which interferes with the incident one. This causes a distortion of both amplitude and phase profiles of the T_e modulation with respect to what would happen without this effect. As χ_e^{amp} and χ_e^{phase} depend on the square of the respective radial derivative of these profiles, they are very sensitive to this effect. The main features of χ_e^{amp} and χ_e^{phase} are reproduced by the empirical model (Fig. 1). Below the threshold $\chi_e^{\mathrm{amp,sim}}$ and $\chi_e^{\mathrm{phase,sim}}$ are small and have comparable values. At the threshold, a jump in $\chi_e^{\mathrm{amp,sim}}$ is observed, stronger for $\alpha = 0.8$ than for $\alpha = 1.0$, due to the different dependencies of q_e on R/L_{T_e}. The model is very simple but indicates clearly that the behavior of the data is compatible with the existence of a threshold. In particular, it reproduces the unusual situation $\chi_e^{\mathrm{amp}} > \chi_e^{\mathrm{phase}}$ which is directly related to the existence of a threshold. It is clear that the exact behavior of the apparent propagation of the heat pulses depends sensitively on the details of the onset of the driven transport just above the threshold. This is reflected by the model which shows that a small change in α has a strong effect on the modulation data. In summary, the behavior of the electron heat flux, the strong change of the experimental heat pulses propagation at $R/L_{T_e} \approx 3$, and GS2 calculations provide convincing evidence for a nonlinear behavior of q_e versus R/L_{T_e}, compatible with the TEM instability under such conditions.

Another important characteristic of TEM modes is their stabilization by collisions. To investigate this question, discharges were run at 600 kA, 2.3 T heated by 0.7 MW of ECH with $\pm 10\%$ power modulation, deposited at a single position $\rho_{\mathrm{ECH}} = 0.38$. In contrast to the above discharges, the line-averaged electron density was not kept constant, but increased in a linear ramp from $\bar{n}_e \approx 2.2 \times 10^{19}\ \mathrm{m}^{-3}$ to $\bar{n}_e \approx 3.7 \times 10^{19}\ \mathrm{m}^{-3}$ during the 2 sec of the ECH. The analyses are carried out in the region $0.4 < \rho < 0.8$. During the density ramp, the local density increases proportionally to the line-averaged value and R/L_n remains constant. Of course T_e, T_i, and their gradients decrease, almost linearly with density, and R/L_{T_e} remains remarkably constant at $10 \pm 5\%$, deduced with accuracy from ECE channels. The value of R/L_{T_i} is estimated to remain constant at about 5 ± 1. We calculated χ_e^{HP} at different time points over time intervals of 150 ms. Here we have the usual situation $\chi_e^{\mathrm{amp}} < \chi_e^{\mathrm{phase}}$. During each of these intervals the variation of density and other plasma parameters is smaller than $\pm 8\%$ around the value in the center of the respective time interval. The profiles of χ_e^{HP} for each time point are shown in the left plot of Fig. 2. Three profiles of χ_e^{PB} during the density ramp are also indicated.

One observes a strong decrease of χ_e^{HP} with increasing density. Towards the end of the density ramp ($\bar{n}_{e19} = 3.2$–3.7) χ_e^{HP} drops below χ_e^{PB}. This effect starts at the plasma edge and propagates towards the center as density increases. It is therefore logical to attribute this to collisionality as shown in the right plot of Fig. 2, which shows $\chi_e^{\mathrm{HP}}/\chi_e^{\mathrm{PB}}$ at 3 values of ρ versus $\nu_{\mathrm{eff}}(\epsilon/\epsilon_{\mathrm{mean}})^{3/2}$, where ϵ is the inverse aspect ratio and ϵ_{mean} the mean ϵ value in the range $0.5 \leq \rho \leq 0.78$. The correction $\epsilon^{3/2}$ is a rough estimate of the dependence of ν_{ei} on ϵ and of the TEM destabilization by ϵ. Indeed, this correction brings the data at the different radii closer to each other compared to the plot using ν_{eff} only (not shown). The normalization by ϵ_{mean} provides a value comparable in magnitude to the range obtained using ν_{eff} in other studies. Figure 2 shows that $\chi_e^{\mathrm{HP}}/\chi_e^{\mathrm{PB}}$ clearly drops below unity over a significant range of collisionality. It must be stressed that the experimental uncertainties are small compared to the observed effect. This is, in particular, due to the good conditions provided for the power balance analysis which is carried out rather close to the deposition of the ECH power and even at high density the electron heat flux remains well defined. The situation $\chi_e^{\mathrm{HP}}/\chi_e^{\mathrm{PB}} < 1$ is unusual: the case $\chi_e^{\mathrm{HP}}/\chi_e^{\mathrm{PB}} = 1$ corresponds to the ideal case of purely diffusive transport with constant χ_e, whereas, in general one finds experimentally $\chi_e^{\mathrm{HP}}/\chi_e^{\mathrm{PB}} > 1$ [22], caused by χ_e dependencies on plasmas parameters, for instance ∇T_e. Figure 3 gives TEM/ITG stability diagrams from GS2

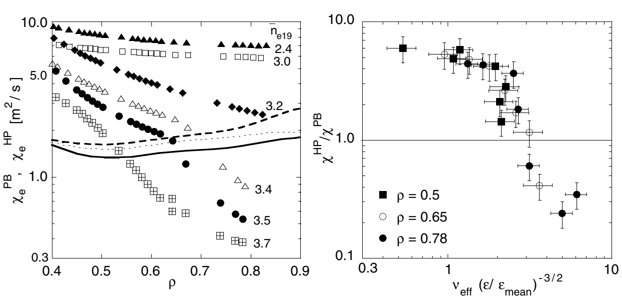

FIG. 2. Left plot: χ_e^{HP} and χ_e^{PB} versus ρ for different values of $\bar{n}_e$ in $10^{19}\ \mathrm{m}^{-3}$ indicated in the plot. The symbols show χ_e^{HP} and the lines χ_e^{PB}, which decreases with $\bar{n}_e$ for the 3 values 2.5, 3.3, and $3.7 \times 10^{19}\ \mathrm{m}^{-3}$. Right plot: Ratio $\chi_e^{\mathrm{HP}}/\chi_e^{\mathrm{PB}}$ versus normalized ν_{eff}.

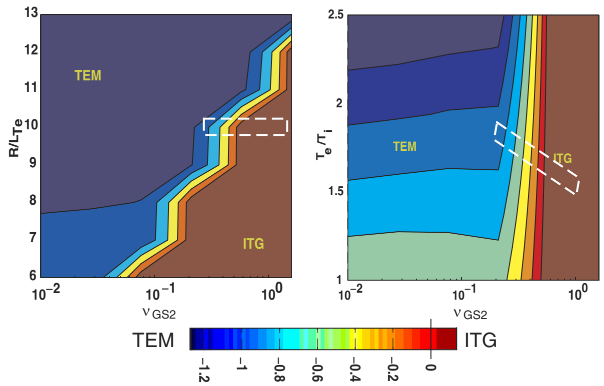

FIG. 3 (color online). Stability diagrams for TEM and ITG showing contours of the mode frequency—positive for ITG, negative for TEM, versus the collisionality used in GS2. In the left plot $T_e/T_i = 1.8$, in the right plot $R/L_{T_e} = 10$. The range of the experiment is indicated by the dashed polygons.

calculations including the experimental range. It shows that the dominant mode changes from TEM to ITG with increasing collisionality, the role of T_e/T_i being weak compared to that of collisions.

Therefore, q_e is TEM dominated at the beginning of the density ramp and ITG dominated at the end. In the upper plots of Fig. 4 we show for each of the two situations the dependence of q_e and q_i as R/L_{T_e} is scanned in GS2 calculations. In each of the two scans all other parameters (including T_e) were kept fixed at their corresponding experimental values.

The results show $q_e > q_i$ in the TEM case and $q_e < q_i$ in the ITG case. The dependence of q_e upon R/L_{T_e} differs significantly in the two cases. For the TEM-driven case q_e increases monotonically with R/L_{T_e}. For the ITG-driven case q_e increases weakly and levels off in the range

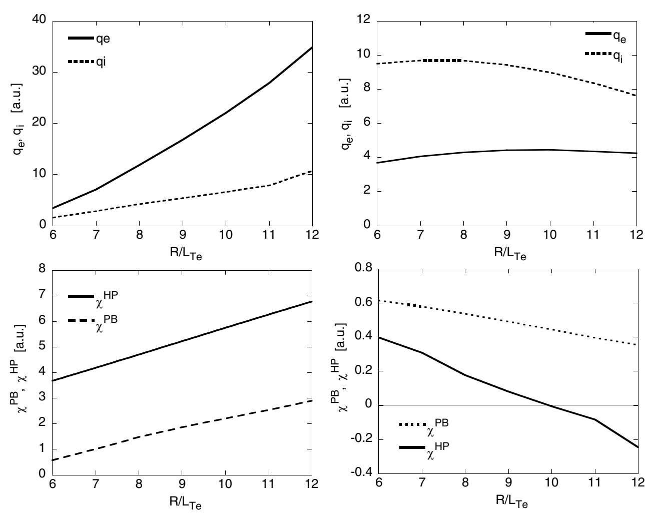

FIG. 4. Upper plots: Electron and ion heat fluxes from the GS2 calculations versus R/L_{T_e} in the TEM-dominated and ITG-dominated cases. Lower plots: χ_e^{PB} and χ_e^{PB} derived from the curves given in the upper plots. The experimental value of R/L_{T_e} is at about 10.

$R/L_{T_e} \approx 10$, which corresponds to the experimental value. This leads to $\chi_e^{\mathrm{HP}}/\chi_e^{\mathrm{PB}} > 1$ in the TEM case and to $\chi_e^{\mathrm{HP}}/\chi_e^{\mathrm{PB}} < 1$ in the ITG case, as indicated directly by the curves χ_e^{HP} and χ_e^{PB} of the lower plots. The heat fluxes, are calculated following [27] at the maximum of $\gamma/k_\perp^2$ and expected to provide realistic values for the ratios q_e/q_i and $\chi_e^{\mathrm{HP}}/\chi_e^{\mathrm{PB}}$. In summary, experimental studies of electron heat transport in plasmas with dominant electron heating exhibit two main properties expected for TEM-driven transport: existence of a threshold in R/L_{T_e} and stabilization by collisions. Quasilinear gyrokinetic calculations indicate that indeed the observed behavior can be explained by TEM-driven transport at low collisionality, gradually stabilized and replaced by ITG-driven electron heat transport as collisionality is increased.

The authors are very grateful to W. Dorland and M. Kotschenreuther for making the GS2 code available and to F. Jenko for fruitful discussions. The excellent support of the ECRH and ASDEX Upgrade technical staff is warmly acknowledged.

[1] V. Alikaev *et al.*, Plasma Phys. Controlled Nucl. Fusion Res., **3**, 111 (1987).
[2] F. Wagner *et al.*, Phys. Rev. Lett. **56**, 2187 (1986).
[3] G. Taylor *et al.*, Nucl. Fusion **29**, 3 (1989).
[4] T. C. Luce *et al.*, Phys. Rev. Lett. **68**, 52 (1992).
[5] W. Suttrop *et al.*, Plasma Phys. Controlled Fusion **39**, 2051 (1997).
[6] P. Gohil *et al.*, Nucl. Fusion **38**, 425 (1998).
[7] L. D. Horton *et al.*, Plasma Phys. Controlled Fusion **41**, B329 (1999).
[8] H. Urano *et al.*, Nucl. Fusion **42**, 76 (2002).
[9] F. Ryter *et al.*, Plasma Phys. Controlled Fusion **43**, A323 (2001).
[10] F. Ryter *et al.*, Phys. Rev. Lett. **86**, 2325 (2001).
[11] F. Ryter *et al.*, Phys. Rev. Lett. **86**, 5498 (2001).
[12] G. T. Hoang *et al.*, Phys. Rev. Lett. **87**, 125001 (2001).
[13] A. Jacchia *et al.*, Nucl. Fusion **42**, 1116 (2002).
[14] S. Cirant *et al.*, Nucl. Fusion **43**, 1384 (2003).
[15] F. Ryter *et al.*, Nucl. Fusion **43**, 1396 (2003).
[16] X. Garbet *et al.*, Plasma Phys. Controlled Fusion **46**, B557 (2004).
[17] A. G. Peeters *et al.*, Phys. Plasmas **12**, 022505 (2005).
[18] C. Angioni *et al.*, Phys. Plasmas **10**, 3225 (2003).
[19] F. Jenko *et al.*, Phys. Plasmas **8**, 4096 (2001).
[20] J. C. Deboo *et al.*, Nucl. Fusion **45**, 494 (2005).
[21] Y. Camenen *et al.*, Plasma Phys. Controlled Fusion (to be published).
[22] N. J. Lopes Cardozo, Plasma Phys. Controlled Fusion **37**, 799 (1995).
[23] F. Imbeaux *et al.*, Plasma Phys. Controlled Fusion **43**, 1503 (2001).
[24] X. Garbet *et al.*, Plasma Phys. Controlled Fusion **46**, 1351 (2004).
[25] G. V. Pereverzev *et al.*, IPP Report No. 5/98, 2002.
[26] M. Kotschenreuther *et al.*, Comput. Phys. Commun. **88**, 128 (1995).
[27] T. Dannert *et al.*, Phys. Plasmas **12**, 072309 (2005).